J MATER SCI **41** (2006) 4023–4039

# Blast impact response of aluminum foam sandwich composites

RAJAN SRIRAM, UDAY K. VAIDYA*
*Department of Materials Science and Engineering, University of Alabama at Birmingham, Birmingham, AL 35294-4461*
*E-mail: uvaidya@uab.edu*

JONG-EUN KIM
*Department of Mechanical Engineering, University of Alabama at Birmingham, Birmingham, AL 35294-4461*

**Published online:** 7 June 2006

Military and civilian structures can be exposed to intentional or accidental blasts. Aluminum foam sandwich structures are being considered for energy absorption applications in blast resistant cargo containers, ordnance boxes, transformer box pads, etc. This study examines the modeling of aluminum foam sandwich composites subjected to blast loads using LS-DYNA software. The sandwich composite was designed using laminated face sheets (S2 glass/epoxy and aluminum foam core. The aluminum foam core was modeled using an anisotropic material model. The laminated face sheets were modeled using material models that implement the Tsai-Wu and Hashin failure theories. Ablast load was applied using the CONWEP blast equations (*LOAD_BLAST) in LS-DYNA. This paper discusses the blast response of constituent S2-glass/epoxy face sheets, the closed cell aluminum foam core as well as the sandwich composite plate. 

## 1. Introduction

The design of energy-absorbing structures has become increasingly important in recent years because blast threats are encountered in military as well as civilian structures. Sandwich composites made of polymer matrix fiber-reinforced face sheets and foam cores have been used for blast protection of structures [1, 2]. Sandwich composites have high strength and stiffness compared to monolithic solid plates [3]. In recent years, several cost-effective manufacturing processes for polymer matrix composites have emerged, one of them being Vacuum Assisted Resin Transfer Molding (VARTM) [3]. The cores used in previous sandwich composite studies were balsa wood and polymeric foam respectively [1–3]. The advantage of using metal foam is its potential use at high temperatures, less moisture-dependent properties, and moderate to low strain rate sensitivity.

Aluminum foams are being increasingly used in energy-absorbing structures [4, 5]. In the theoretical analysis of aluminum foams for blast amelioration by Ashby *et al.* [4], it was shown that the foam is exploited as an energy absorber by mounting a heavy buffer plate in front of it. The blast impulse first accelerates the buffer plate and the kinetic energy acquired by the plate is dissipated by the foam. This implies that a thicker and heavier plate will have lesser acceleration; hence less kinetic energy has to be dissipated by the foam. The foam should possess a plateau stress just below that of the pressure that the structure can support. For example, if a structure can withstand a pressure of 0.3 MPa, the plateau stress of the foam used should be just under 0.3 MPa.

Experimental, numerical and analytical studies on blast on aluminum foam in the presence and absence of a buffer plate were done by Hanssen *et al.* [6]. In their study it was observed that the use of foam as a sacrificial layer ensures local protection of the structure. The plastic compression of the aluminum foam consumes kinetic energy, which eventually halts the progression of the shock wave produced by the blast. The structural integrity of the panel was maintained when a cover plate was placed in front of

*Author to whom all correspondence should be addressed.
0022-2461 
DOI: 10.1007/s10853-006-7606-4

the foam panel. It was observed that both the cover plate and the foam attained a double/concave curvature when subjected to blast loading. The final depth of deformation on the foam panel relative to its edges was termed "dishing". On the basis of work done by Liang *et al*. [7], Hanssen *et al*. [6] reported that the foam and the cover plate can sustain a higher blast load because of "dishing".

The present work considers a sandwich composite design for blast protection. A sandwich composite consists of fiber reinforced face sheets and an aluminum foam core. The use of the face sheets would be analogous to addition of the cover plate in the studies done in [6]. Xu and Hutchinson [2] modeled the blast on sandwich plates with aluminum core. The core was modeled using a continuum constitutive law for aluminum foam [8]. The top and bottom face sheets were modeled using the von Mises criterion. It was shown in their study that the face sheets with sufficiently strong core have the potential to sustain larger impulses compared to solid plates of the same material and weight.

The impact resistance and energy absorption of sandwich composites with aluminum foam and polymer matrix fiber-reinforced face sheets was studied by Vaidya *et al*. [9]. They reported that energy absorption and failure strongly depended on the type (e.g. S2-glass, Kevlar, carbon and E-glass) and the property of the face sheets. The aluminum foam sandwich composites used in their study were produced by the VARTM process. The face sheets made of S2-glass and Kevlar were seen to possess superior impact resistance and energy absorption compared to carbon and E-glass fiber reinforcements. The face sheets with higher compressive strength and heavier tow (such as Kevlar and S2-glass) were effective in spreading the load over a larger area of the underlying core. In the present work a blast load and damage progression on an aluminum foam sandwich composite plate with S2-glass face sheets has been simulated using LS-DYNA.

## 2. Mechanical property of aluminum foam

A Cymat closed cell aluminum foam was used in this study [10, 11]. The Cymat foam is anisotropic and is produced by the gas injection process [10, 11]. The uniaxial compression characteristics of closed cell foams have been analyzed in [4]. The stress-strain behavior of aluminum foam is represented by three stages namely, linear elastic, plastic collapse and densification as shown in Fig. 1. In the first stage, the response of the aluminum foam is linear elastic for small strains, and is controlled by three different strains; i.e. bending of cell edges, compression of gases trapped in the cells, and stretching of cell walls. In the second stage, the stress plateau ($\sigma_{pl}$) represents cell collapse and the strain is not recoverable in this region. This property becomes important for foams when used for energy absorption applications. It can be observed that the stress plateau is serrated, which occurs

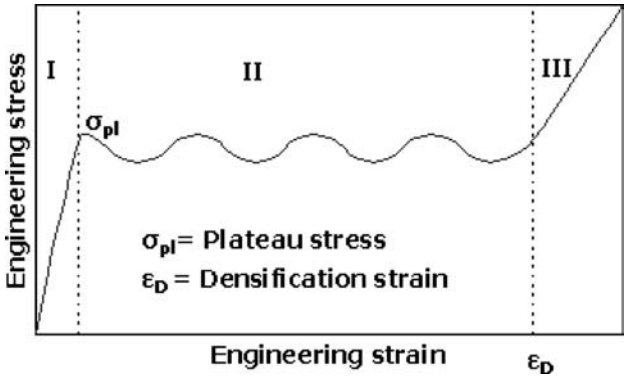


*Figure 1* Mechanical response of Cymat [11] aluminum foam under compressive loading.

because of the brittle nature of the Cymat foam. The serrations correspond to fracture of cell walls. In the third stage, densification of the foam takes place. The strain at which the densification starts is known as 'densification strain' ($\varepsilon_D$) and for Cymat aluminum foam the densification strain is around 0.65–0.68 [12]. In case of uniaxial tension, the foam exhibits brittle fracture and the failure strain is around 0.0017 [12]. The tensile strength of aluminum foam is less than its compression strength due to different failure mechanisms, i.e. local fracture in tension and buckling in compression [13]. In the case of uniaxial shear, the failure strain of the aluminum foam is approximately 0.002 [11].

In the study of dependence of material distribution on modulus of aluminum foams [14], it was found that the material distribution does not have significant effect on modulus. The fracture behavior of aluminum foam was investigated in [15] and the crack propagation in aluminum foam was determined to be a diffuse, stochastic process because of spatial variability in the morphology and properties of the cell walls. Small cracks, fully contained within a single wall of a closed cell propagate at a critical energy release rate. Large cracks become more diffuse, resulting in intact cell walls in the wake [15]. It was illustrated in [16] that Cymat aluminum foam does not show strong rate dependence for strain rates between $10^{-3}$ to $10^{3}$/s.

## 3. Blast simulation

Blast is an extraordinary type of dynamic load. There can be two types of blast; internal and external. Internal blast occurs because of detonation of high explosives, or on accumulation of flammable gas/air mixtures, while external blast occurs because of high explosives or atomic explosions. The blast phenomenon is discussed by Beshara [17]. In the process of an explosion the blast travels as an incident wave until it strikes an object. Upon striking the object, a reflected wave is generated which travels back towards the point of explosion. At a point, some distance

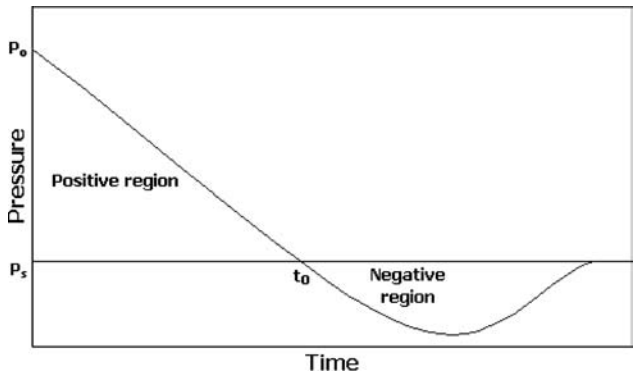


*Figure 2* Characteristics of blast load.

from the explosion center, the reflected wave meets the incident wave, producing a single vertical wave front called a "Mach Stem". The structure below the point of intersection of the reflected wave and the incident wave experiences a single shock, whereas the surface above this point experiences a shock history which is a resultant of the incident and reflected wave.

The pressure versus time plot of a typical blast wave is shown in Fig. 2. The pressure builds up to a peak value of the overpressure ($P_o$). The pressure then decays to local ambient pressure $P_s$ ambient in time ($t_0$) to a partial vacuum of very small amplitude and eventually returns to ($P_s$). The portion of the pressure-time history below zero is called the "negative or suction phase" and the portion above zero is called the "positive phase". In most blast studies the negative phase of the blast wave is ignored, and only the parameters associated with the positive phase are considered because the damage to the structure is caused by the "positive phase".

In the positive phase the pressure at any time ($t$) is described in terms of the peak overpressure ($P_o$), the dimensionless wave form parameter ($\alpha$), and the positive phase duration time ($t_0$). These parameters are linked by Friedlander's equation given by Equation 1. The impulse per unit of projected area is given by Equation 2.

$$P(t) = P_o\left(1 - \frac{t}{t_o}\right)\exp\left(-\alpha\frac{t}{t_o}\right) \tag{1}$$

$$I_s = \int_0^{t_0} P(t)dt = P_0 t_0\left[\frac{1}{\alpha} - \frac{1}{\alpha^2}(1 - \exp(-\alpha))\right] \tag{2}$$

The overpressure of mass-detonating materials such as nuclear weapons can be modeled by relating their effective mass to an equivalent mass of Tri-Nitro-Toluene (TNT). Blasts from chemical explosions of flammable hydrocarbons can also be modeled by considering an equivalent mass of TNT [17]. The blast characteristic of any given mass of TNT can be obtained with respect to a known referenced mass of TNT using a blast scaling law [17]. The law states that "when two charges of the same explosive and same geometry, but of different size are detonated in the same atmosphere, the shock waves produced are similar in terms of the same scaled distances". The scaled distance ($Z$) is expressed in terms of distance $R$ from the center of explosion and weight of explosive ($W$) as shown in Equation 3. The scaling law can also be applied to time parameters. The relation between the scaled time ($t_{sc}$) in terms of given time is given in Equation 4. The decay parameter ($\alpha$) and peak overpressure ($P_o$) are not scaled, but the values that correspond to the scaled distance are used.

$$Z = R/W^{1/3} \tag{3}$$

$$t_{sc} = \frac{t}{W^{1/3}} \tag{4}$$

### 3.1. LOAD_BLAST

The LOAD_BLAST function developed in [18] incorporates the CONWEP algorithm [19]. CONWEP is an implementation of empirical blast model obtained in studies of Kingery and Bulmash [20]. The pressure load ($P$) is given in terms of normal incidence pressure ($P_1$), side-on incidence pressure ($P_2$) and angle of incidence ($\theta$) given by Equation 5. The resultant pressure load accounts for normal incidence and oblique incidence respectively.

$$P = P_1\cos^2\theta + P_2(1 - \cos\theta)^2 \tag{5}$$

It can be observed from Equation 5 that at normal incidence, i.e. ($\theta = 90^\circ$) the value of the pressure load $P$ is $P_2$. A typical pressure time history at 10 cm increments of radial distance from the center is shown in Fig. 3. It can be observed that the center experiences highest pressure load which continues to decrease away from the center. Similarly, the time at which the corresponding locations experience maximum load is different.

The LOAD_BLAST function incorporates Friedlander's equation (Equation 1) and Hoffman's scaling law (Equation 3) to calculate the pressure load for a given mass of TNT at a given distance.

To understand the variation of pressure with amount of TNT and distance, two studies were conducted. In the first

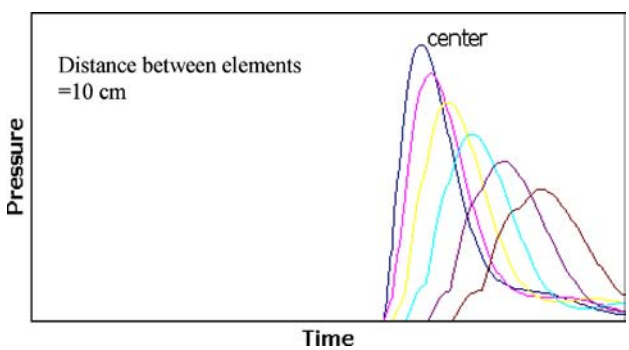


*Figure 3* Pressure vs. time for a sample at different distance from center.

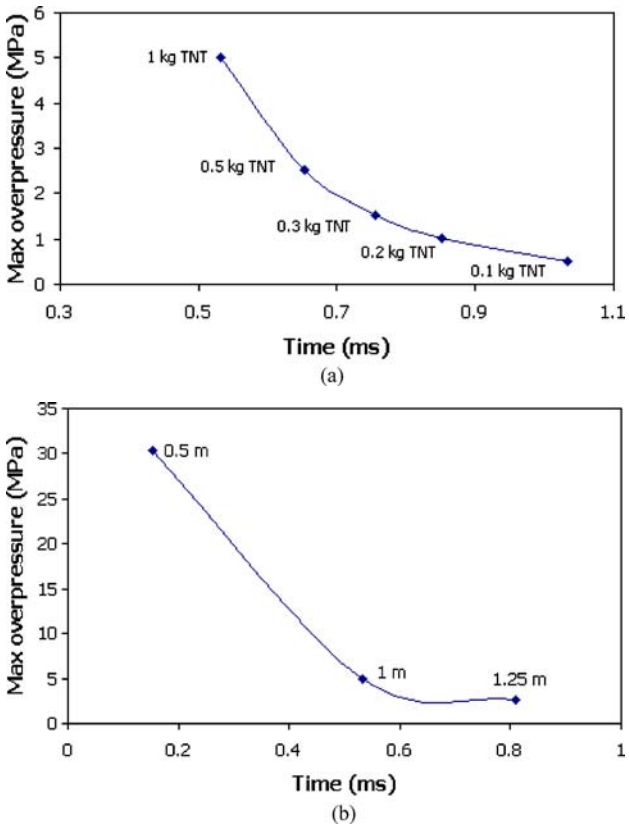


*Figure 4* (a) Maximum overpressure vs. time of maximum overpressure (constant distance = 1 m). (b) Maximum overpressure and time of maximum overpressure (constant load = 1 kg TNT).

study, the amount of TNT was kept constant as shown in Fig. 4a. It can be seen that as the amount of TNT decreases, the time at which the blast reaches the structure increases, following a third degree polynomial fit. In the second study, the distance of the blast was kept constant and the amount of TNT was varied as shown in Fig. 4b. It was found that pressure increases exponentially when the distance is reduced.

## 4. Simulation details

Material models which closely approximate the behavior of Cymat aluminum foam and S2-glass/epoxy laminates were adopted in this work. Material model 126 was used for the aluminum foam because this material model adequately accounts for the anisotropic characteristics of the aluminum foam [21, 22]. Material models 59 and 161 were used to simulate the face sheets. Material model 59 implements the Tsai-Wu [23] failure criterion, and material model 161 implements Hashin's [24] failure for solid elements. The blast load was applied using the *LOAD_BLAST function in LS-DYNA. The material axis for the aluminum foam and face sheets was defined using AOPT [25].

TABLE I. Material property of S2-glass/epoxy for material model 161 [26]

| | |
|---|---|
| $\rho = 1783\,\text{kg/m}^3$ | $E_x = E_y = 24.1$ GPa, $E_z = 10.4$ GPa |
| $G_{xy} = G_{yz} = G_{zx} = 5.9$ GPa | $\nu_{xy} = 0.12$, $\nu_{yz} = \nu_{zx} = 0.4$ |
| $\varphi = 40^\circ$ | $X_T = Y_T = 0.59$ GPa, $Z_T = 69$ MPa |
| $X_C = Y_C = 0.35$ GPa | $S_{FC} = 0.69$ GPa, $S_{FS} = 0.55$ GPa |
| $S_{xy} = S_{yz} = S_{zx} = 48.3$ MPa | |

### 4.1. Blast impact on face sheet

The properties for the S2-glass/epoxy face sheets [26] used as input to the material model 161 are listed in Table I. The value of fiber crush strength ($S_{FC}$) and fiber shear strength ($S_{FS}$) used in the simulation were 0.69 GPa and 0.55 Gpa, respectively. The coefficient of 0.1 was used to define the strain rate dependant properties. After compressive fiber failure, the strength of the fiber and matrix are reduced to the residual strength values given by $S_{xCR}$ and $S_{yCR}$, respectively.

The input values for material model 59 are provided in Table II. The bulk modulus was calculated using rule of mixtures given by Equation 6 in terms of fiber volume fraction ($V_{\text{fiber}}$), matrix volume fraction ($V_{\text{matrix}}$), elastic modulus of fiber ($E_{\text{fiber}}$), and elastic modulus of matrix ($E_{\text{matrix}}$). In this case, a 50% $V_{\text{fiber}}$ was assumed.

$$\frac{1}{(KF)} = \frac{V_{\text{fiber}}}{E_{\text{fiber}}} + \frac{V_{\text{matrix}}}{E_{\text{matrix}}} \tag{6}$$

Two unidirectional face sheets each of dimension 0.3 m × 0.3 m × 0.0015 m were modeled using 2500 elements. Constant stress element formulation was used because material model 161 can be modeled only with constant stress element formulation. The face sheets were fully fixed for all degrees of freedom as shown in Fig. 5. ERODING SINGLE SURFACE was selected to define contact surface between the layers of the face sheet [27]. A simulation was conducted assuming that 0.4 kg of TNT was placed 1 m away from the material. This condition produced a 2.1 MPa pressure load as shown in Fig. 6a. From the figure, it may be noted that the pressure has a radial pattern. The radial pattern can also be illustrated using the output obtained for the elements as shown in Fig. 6b.

The convergence for the simulation was checked as follows. The blast load was applied on a single face sheet that was fully fixed at the corners. The number of elements was increased from 100 to 2500 for a blast load magnitude

TABLE II. Material property of S2-glass/epoxy for material model 59

| | |
|---|---|
| $\rho = 1783\,\text{kg/m}^3$ | $E_x = E_y = 24.1$ GPa, $E_z = 10.4$ GPa |
| $\nu_{xy} = 0.12$, $\nu_{yz} = \nu_{zx} = 0.4$ | $G_{xy} = G_{yz} = G_{zx} = 5.9$ GPa |
| KF = 27.1 GPa | $X_T = Y_T = 0.59$ GPa, $Z_T = 69$ MPa, |
| $X_C = Y_C = 0.35$ GPa, $Z_C =$ | $S_{xy} = S_{yz} = S_{zx} = 48.3$ MPa |

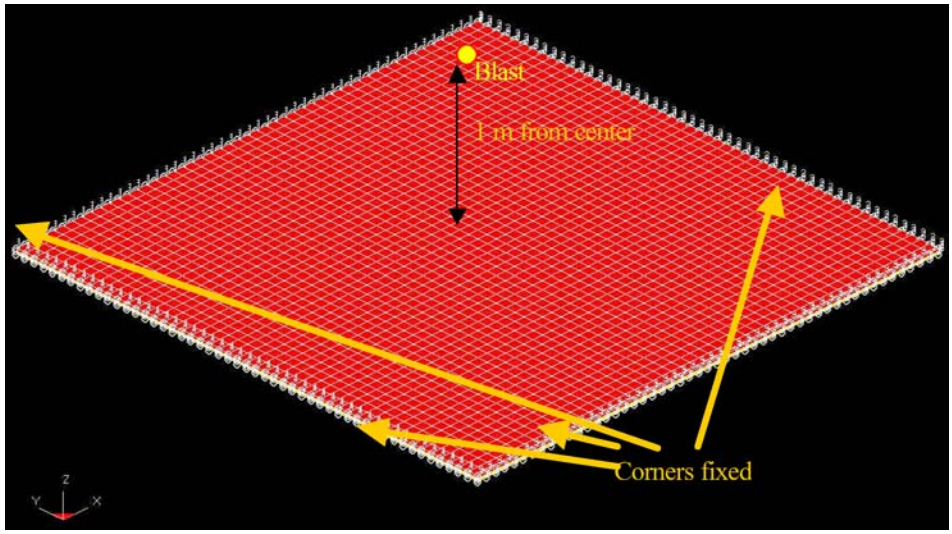


*Figure 5* Laminates restricted for all degrees of freedom along the sides.

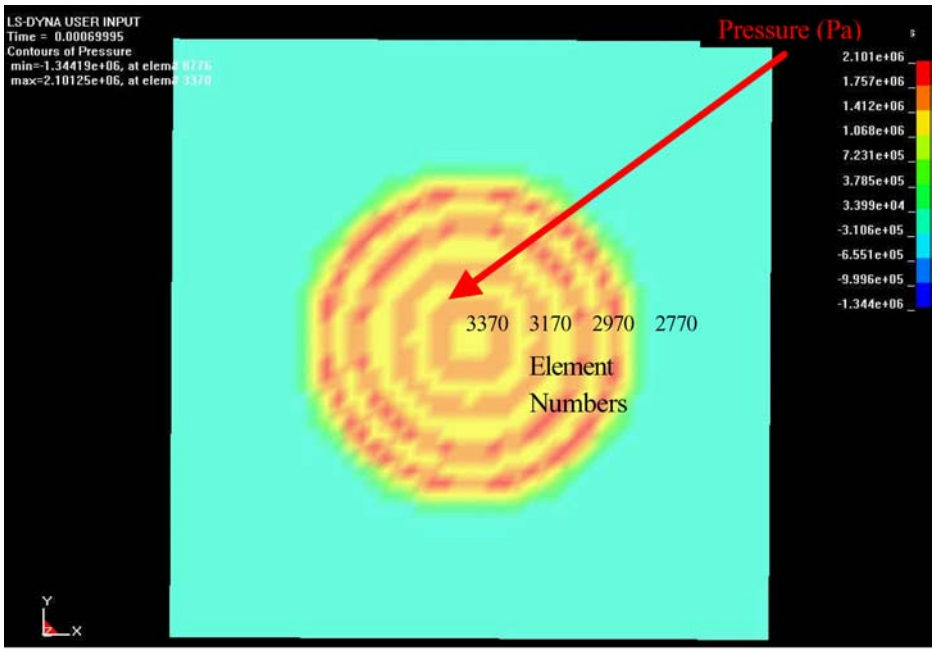


(a)

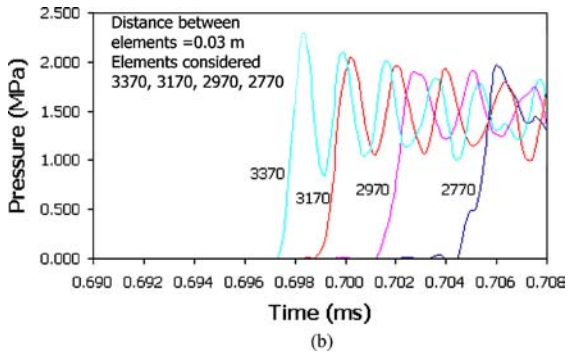


(b)

*Figure 6* (a) Showing radial pattern and maximum pressure of 2.1 MPa (The values on the scale are in MPa). (b) Element wise representation of radial pattern.

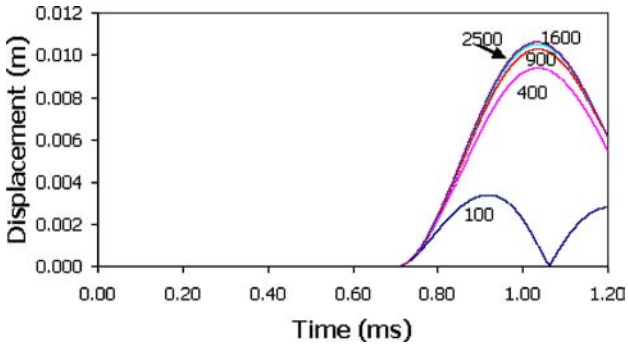


*Figure 7* Convergence of results when the number of elements was increased from 100–2500.

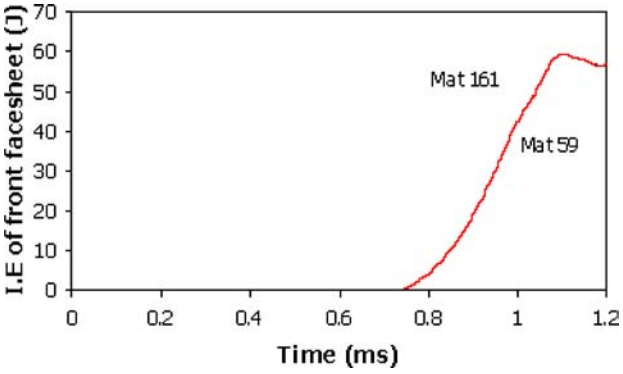


*Figure 8* Internal energy (I.E.) of the front face sheet exposed to blast load of 2.1 MPa.

of 2.1 MPa. As shown in Fig. 7, the displacement of the face sheet did not change based on the number of elements for 1600 to 2500 elements. Hence, each face sheet was modeled using 2500 elements.

The internal energy of the front face sheet was used to compare the results for material models 59 and 161, respectively. From Fig. 8 it can be observed that the behavior of both the models is nearly the same. This can be explained on the basis of the constitutive equations used in these material models. Material model 59 uses the yield/failure theory based on the Tsai-Wu theory [23], and material model 161 uses yield/failure theory which is based on Hashin's theory [24]. Both these material models can be used to predict the behavior of unidirectional composites, but using material model 161, the failure modes are predicted [24].

The failure modes obtained from using material model 161 are shown in Figs 9a–d. These failure modes were obtained by plotting the history variables [22] of material model 161. To visualize the failure modes, the blast load was increased from 2.1 MPa to 5 MPa. For all the failure modes, values $\geq 1$ indicate failure. The sites of shear failure, compressive failure, matrix cracking, and delamination at time 0.95 ms are shown in Figs 9a–d, respectively. Transverse shear failure is seen at the corners only in the

TABLE III. Material property of foam for material model 126

| | |
|---|---|
| $\rho = 300\,\text{kg/m}^3$ (15% relative density) | $E = 72$ GPa |
| $\nu = 0.33$ | $\sigma_y = 145$ MPa |
| $E_{xxu} = 300$ MPa, $E_{yyu} = 460$ MPa, $E_{zzu} = 575$ MPa | $G_{xyu} = G_{yzu} = G_{zxu} = 1000$ MPa |
| TSEF = 0.002 | SSEF = 0.003 |

fiber direction and failure is not observed in the direction perpendicular to the fiber (Fig. 9a). Compressive fiber failure is observed at the corners where the laminate was restricted for all degrees of freedom (Fig. 9b). Matrix crack occurs at sites wherever the face sheet undergoes buckling (Fig. 9c). Delamination is observed over the whole face as shown in Fig. 9d. The delamination is attributed to the separation of the interface between the fiber and the matrix, which is considered by incorporating Coulomb-Mohr theory in material model 161. The Type-4 hourglass option, which uses stiffness stabilization was adopted. A rule of thumb that hourglass energy should be less than 10 percent of internal energy was used to check that hourglass modes were eliminated from the simulation.

## 4.2. Blast impact on foam

The properties for the aluminum foam are listed in Table III [11]. The elastic moduli in three different direction for the uncompressed configuration are given by $E_{xxu}$, $E_{yyu}$, and $E_{zzu}$. The shear moduli for the uncompressed configuration are given by $G_{xyu}$, $G_{yzu}$, and $G_{zxu}$. After compression, the foam is treated as an isotropic material, and the property of aluminum in a compressed configuration is represented using elastic modulus ($E$), yield stress ($\sigma_y$), and Poisson's ratio ($\nu$). The tensile strain to failure (TSEF) and the shear strain to failure (SSEF) signify that any element that has tensile strain greater than TSEF or shear strain greater than SSEF will be removed from further calculation. The uniaxial compression stress-strain and shear stress-strain curves used to represent the foam in uncompressed configuration are shown in Figs 10a and 10b, respectively.

The foam of dimension 0.3 m $\times$ 0.3 m $\times$ 0.0159 m was modeled using 7500 elements. It was restricted for all degrees of freedoms along the corners as shown in Fig. 11. Co-rotational element formulation 0 was used. A blast load of 5 MPa was applied to the foam which resulted in a pressure pattern as shown in Fig. 12. The elements along the corners eroded as shown in Fig. 13. Recalling the case of the face sheet (Fig. 9a) the shear mode failure occurred along the corners. The foam along the corners undergoes shear or tensile failure because SSEF and TSEF of the foam is small, i.e., 0.003 and 0.002 respectively. Type-2 hourglass option which uses viscous forces for stabilization was used for modeling the aluminum foam.

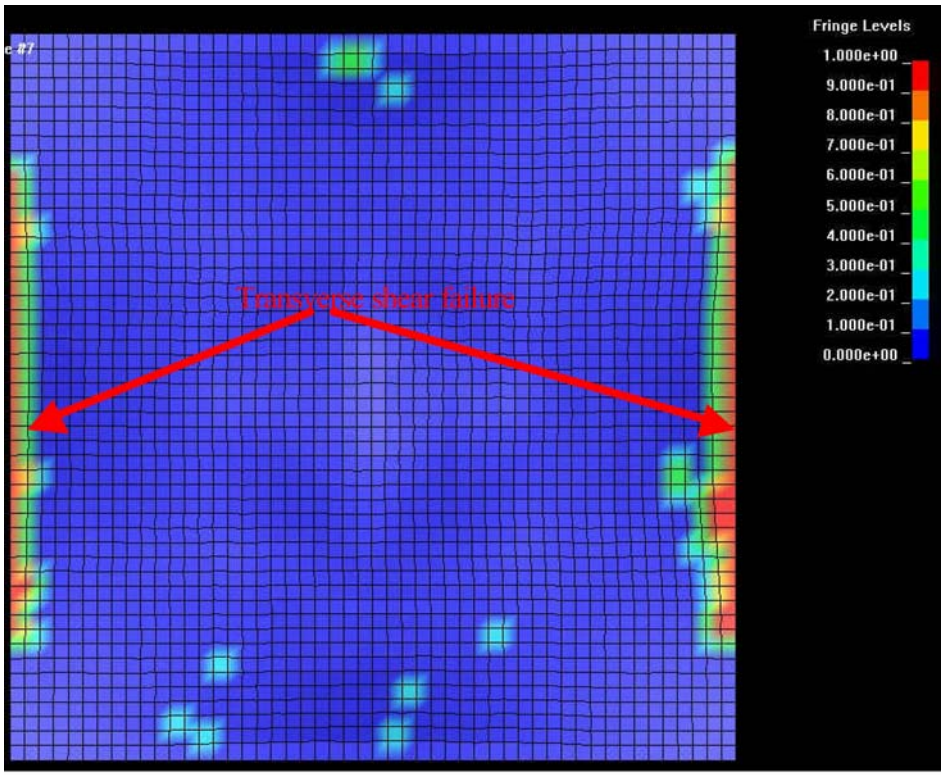


(a)

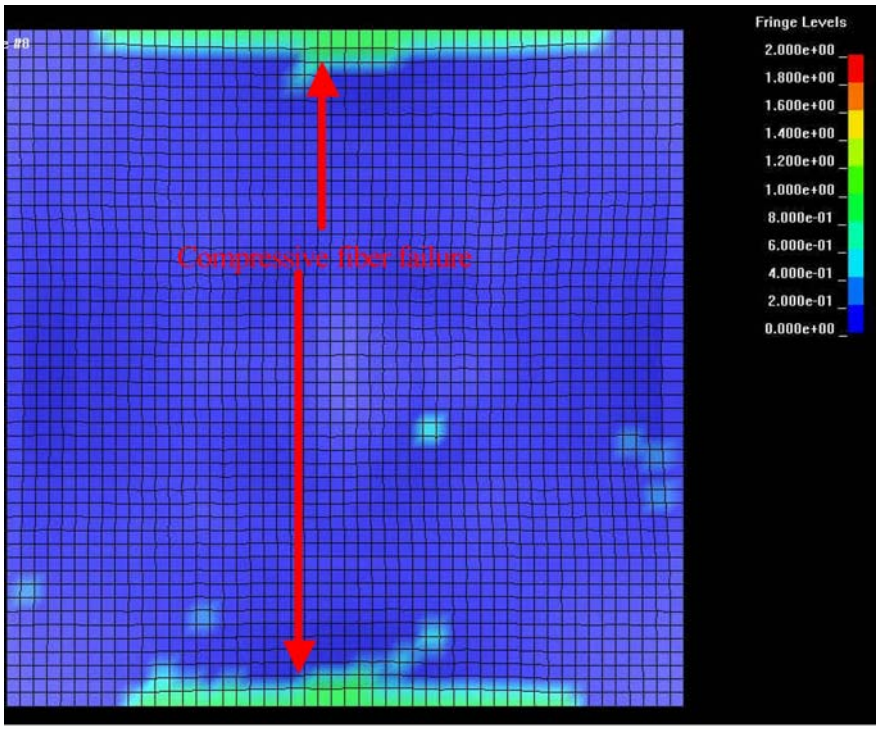


(b)

*Figure 9* (a) Tensile/shear failure in fiber at blast load of 5 MPa (0 = elastics & 1 = failed). (b) Compression failure in fiber blast load of 5 MPa (0 = elastics & 1 = failed). (c) Matrix crack blast load of 5 MPa (0 = elastics & 1 = failed). (d) Delamination blast load of 5 MPa (0 = elastics & 1 = failed).
(*Continued on next page*)

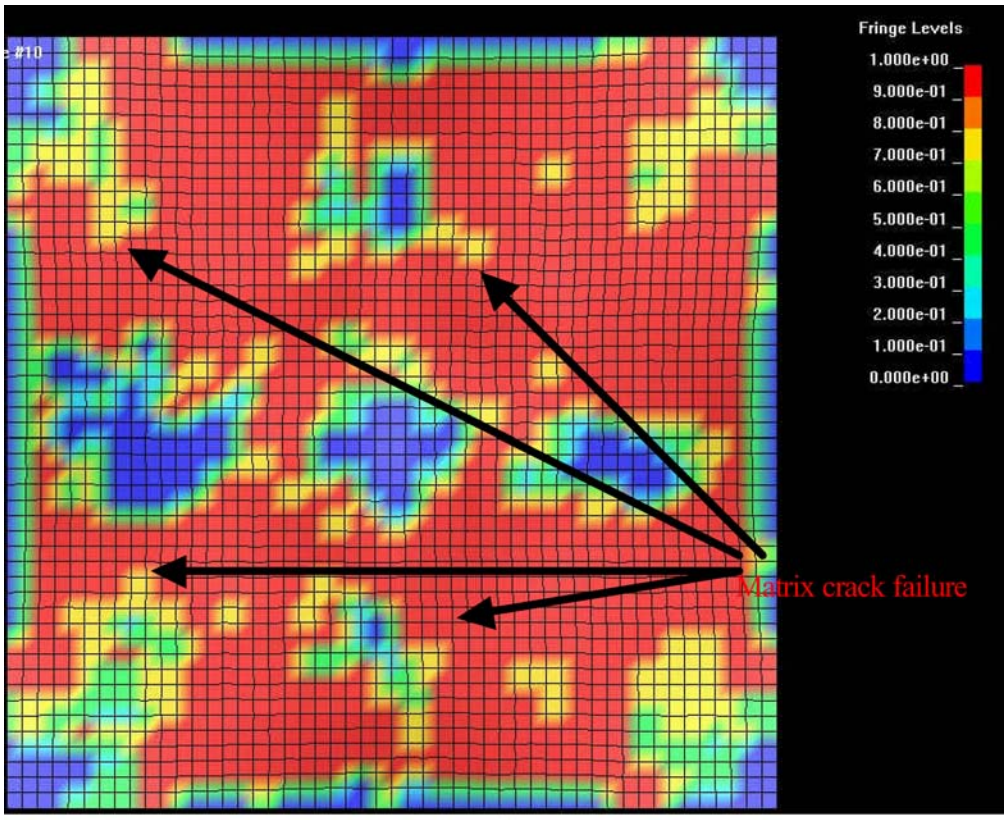


(c)

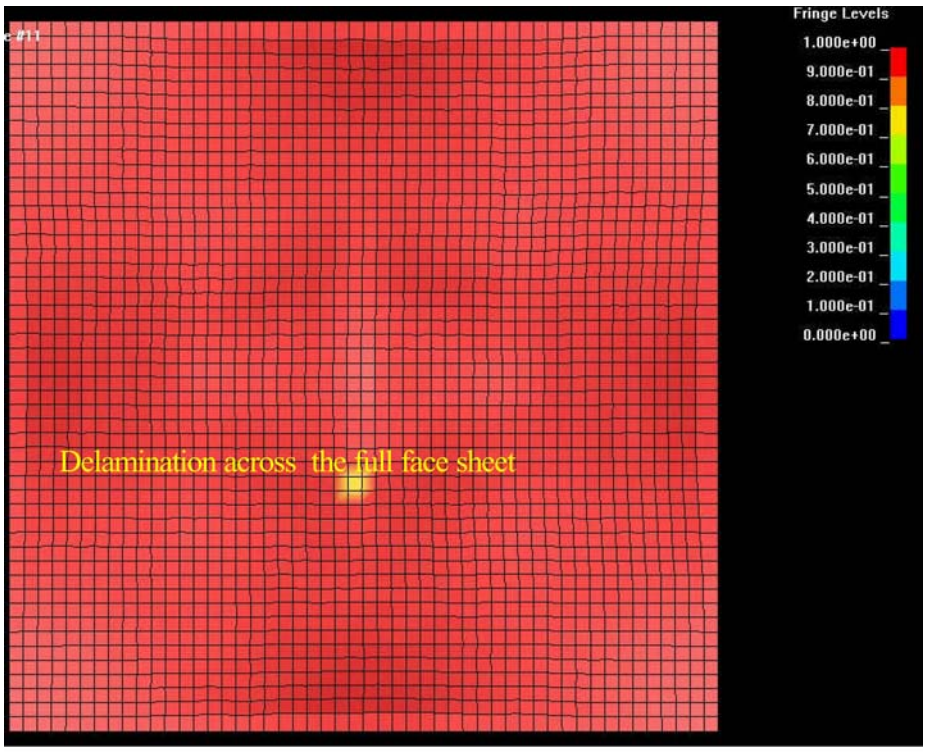


(d)

*Figure 9* (Continued)

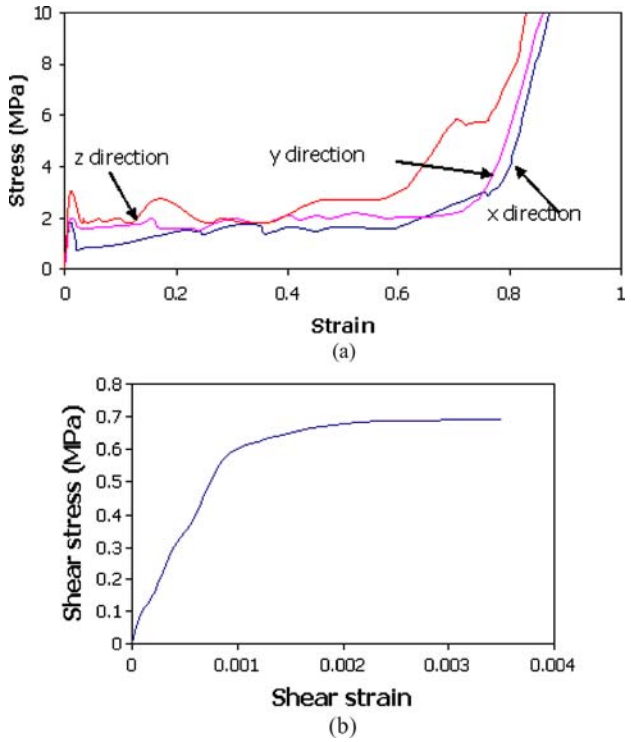


*Figure 10* (a) Compressive stress-engineering strain of aluminum foam in three directions. (b) Shear stress-engineering strain of aluminum foam in three directions.

### 4.3. Blast impact on sandwich composite

The sandwich plate was modeled considering two S2-glass/epoxy face sheets on either side of the foam core as shown in Fig. 14. The dimensions of the foam and face sheet were 0.3 m × 0.3 m × 0.0159 m and 0.3 m × 0.3 m × 0.0015 m respectively. The face sheets were modeled using material model 161. The foam was modeled using material model 126 with corotational element formulation 0. The sandwich composite was restricted for all degrees of freedom along the corners as shown in Fig. 14. ERODING SURFACE TO SURFACE was used to define between face sheet and foam core. ERODING SINGLE SURFACE was selected to define the contact surface between the face sheets layers.

The blast impulse is converted into impulse of the first face sheet which in turn is converted into the impulse of the subsequent face sheet and so on (Fig. 15). The impulse is then transferred to the foam. The impulse acquired by the foam is dissipated by crushing of the foam cells. These findings are analogous to those reported in [6] that demonstrated the conservation of momentum/impulse transfer with the steel plate.

The momentum of the face sheets and the foam were considered for different magnitudes of the blast load. The TNT charge was placed 1 m away from the sandwich composite and the amount of charge was varied. The amounts of TNT considered were 0.1 kg, 0.3 kg, 0.5 kg and 1 kg respectively. The peak pressures attained for the different charge magnitudes are shown in Fig. 5a. The variation of resultant momentum versus time for different blast loads is shown in Figs. 16a–d. It may be noted that the plots have different axes.

It can be observed from Figs 16a–d that the momentum of the foam reaches a plateau. The plateau may be attributed to the crushing of the foam. In material model 126 the anisotropic material behavior changes to isotropic following densification. The curve of the resultant momentum shifts as the blast wave progresses from the top layer to the inner layers (Face sheet1 to Face sheet2 and so on), as shown in Fig. 15. This shift occurs when failure is observed in Face sheet1.

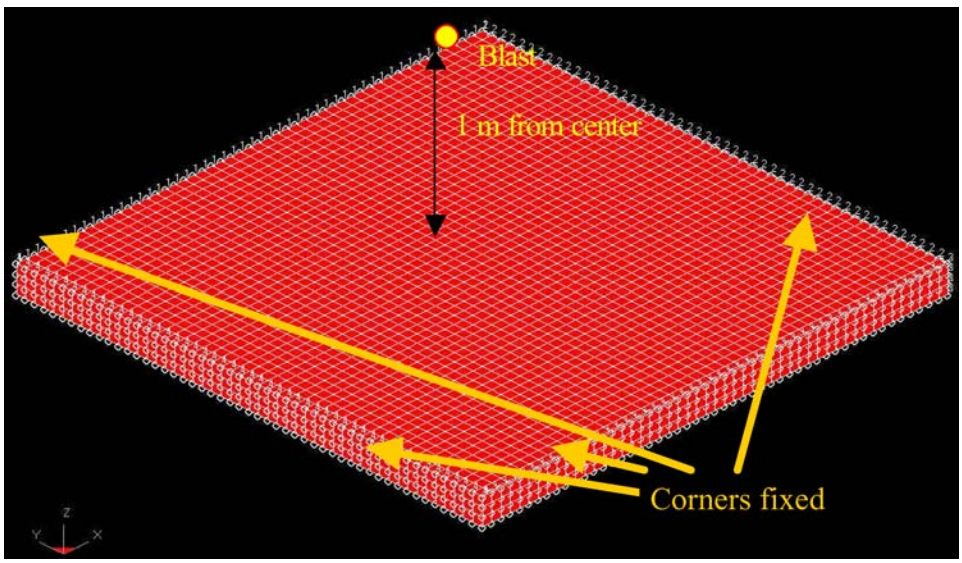


*Figure 11* Foam restricted for all degrees of freedom along the corners.

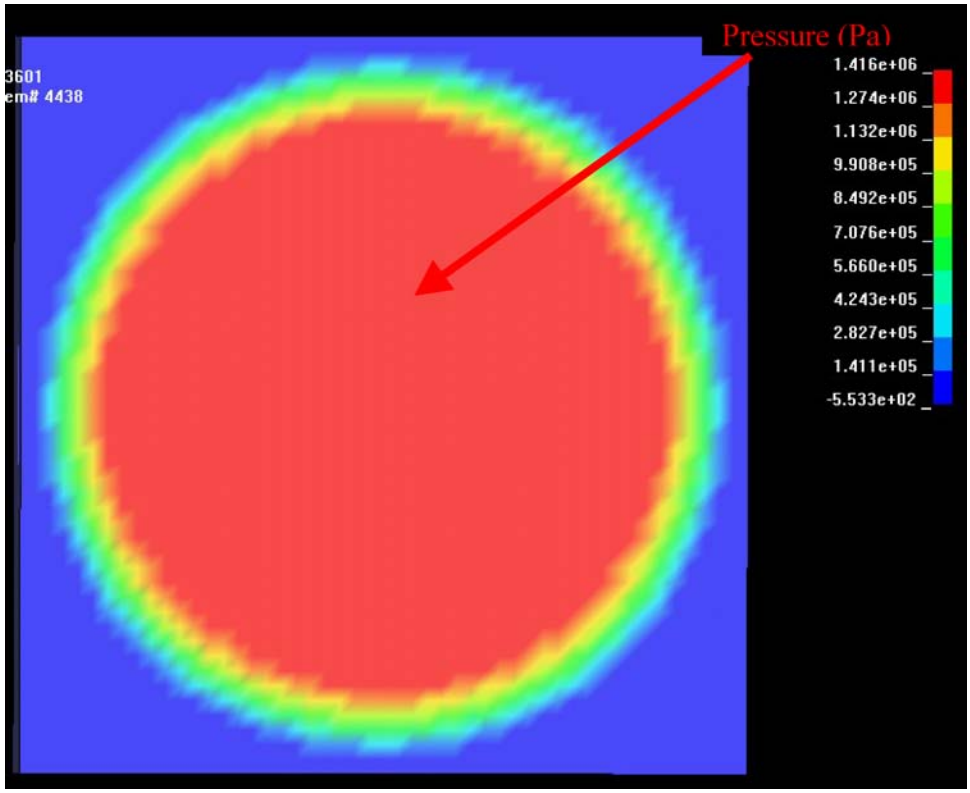


*Figure 12* Radial pattern of pressure observed in the foam at blast load of 5 MPa.

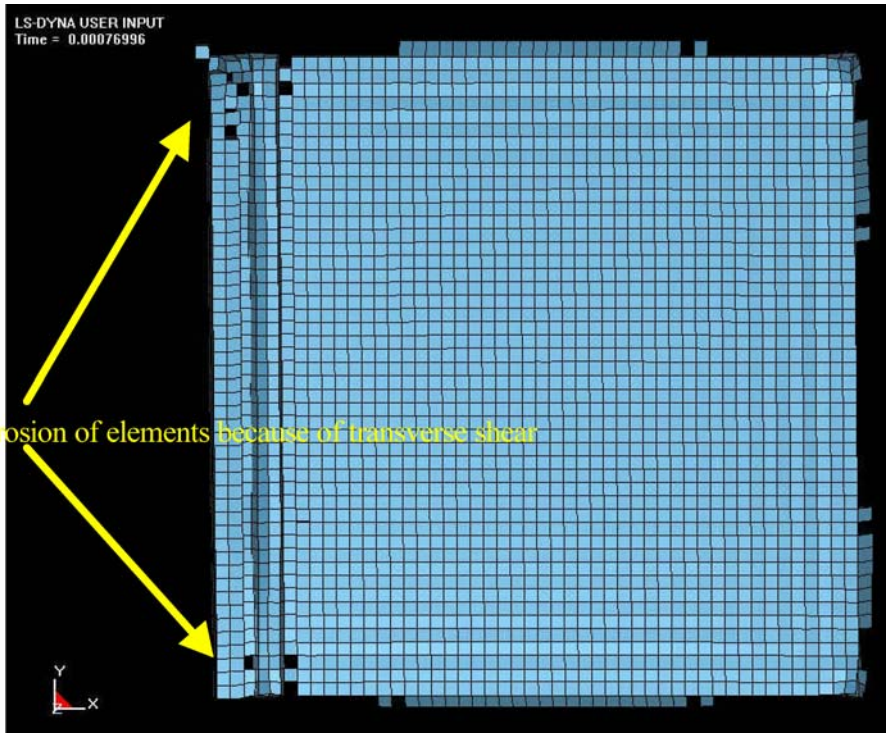


*Figure 13* Fracture observed along the corners of the foam.

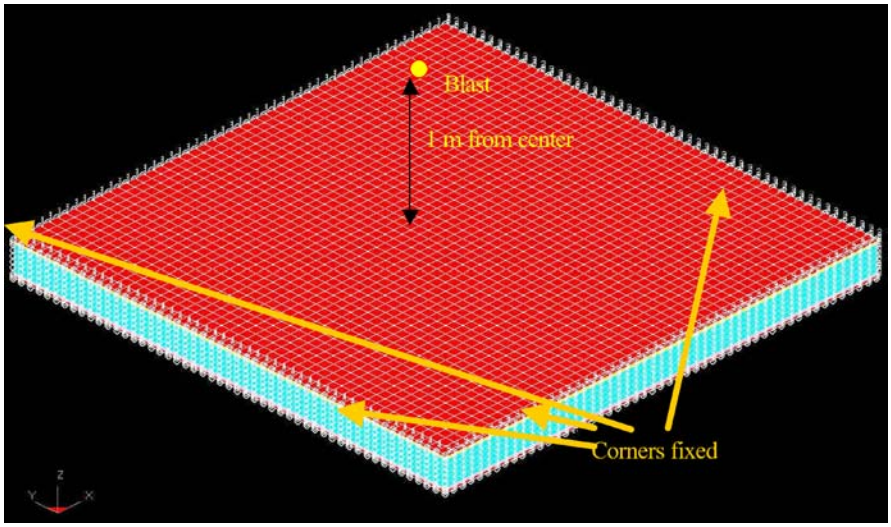


*Figure 14* Sandwich composite restricted for all degrees of freedom along the corners.

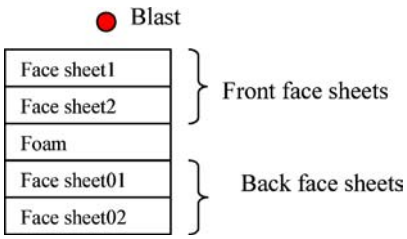


*Figure 15* Schematic representation of the sandwich composite in relation to the blast source.

The failure of the sandwich composite is shown in Fig. 17. Some elements in the foam have fractured. Two failure strains, namely TSEF and SSEF were used in defining the input parameters of the material model 126 for the foam. The eroded elements were observed to have exhibited either tensile or shear failure. Beals *et al*. [28] showed that the aluminum foam core goes into shear loading. Gioux *et al*. [29] argued that loading in the aluminum foam core should not be considered as shear loading but as a case of multiaxial load. So it cannot be said conclusively that the aluminum foam core is completely under shear in the

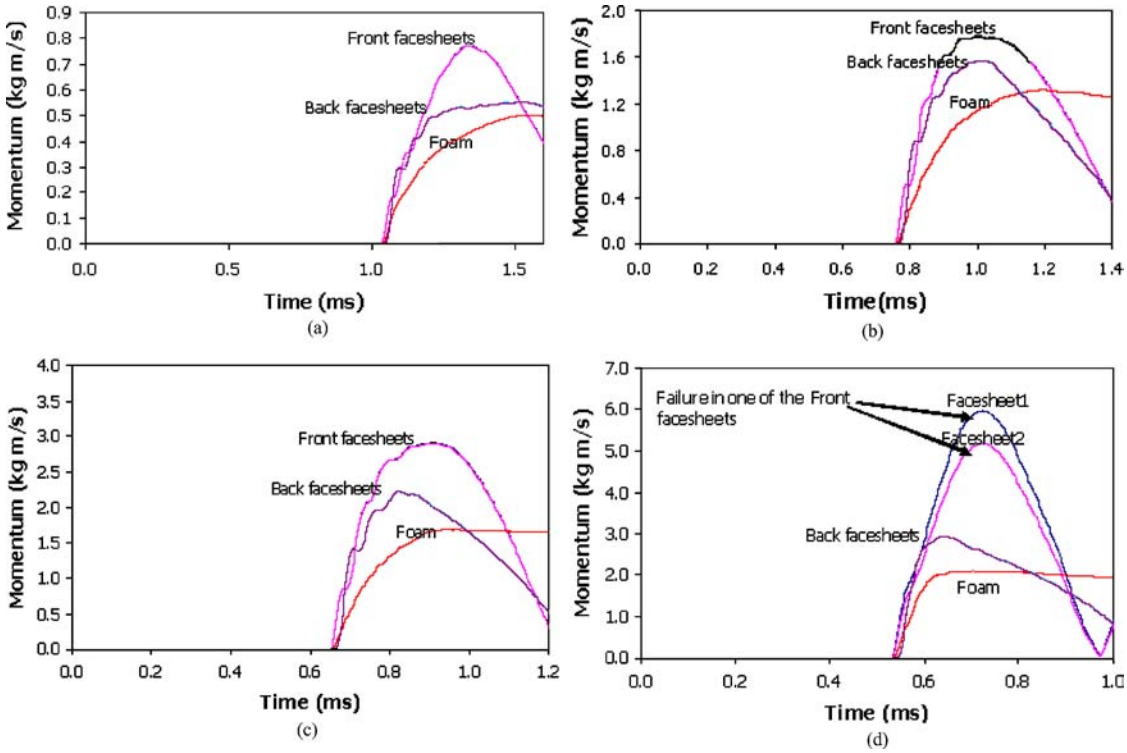


*Figure 16* (a) Momentum of face sheets and foam (TNT = 0.1 kg). (b) Momentum of face sheets and foam (TNT = 0.3 kg). (c) Momentum of face sheets and foam (TNT = 0.5 kg). (d) Momentum of face sheets and foam (TNT = 1 kg).

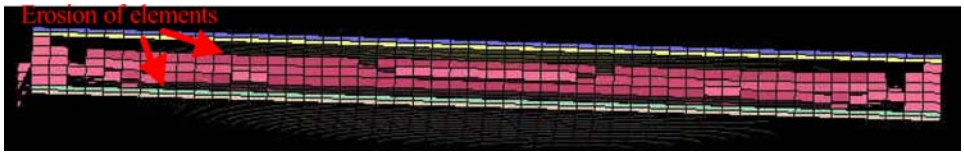


*Figure 17* Blast impact on sandwich composite at time of 1 ms, blast load = 5 MPa.

present case, but it can be argued that the region where erosion of elements were observed is shear dominated because the sandwich composite is under compressive load.

Shear mode failure, compressive mode failure, matrix cracking and delamination all of which were observed in the top face sheet as shown in Figs 18a–d respectively. Shear mode of failure is seen at the middle and in the edges or corners (Fig. 18a). Strain localization due to stretching and transverse shear was observed at the corners of the top face sheet also by studies in [2] when they modeled the face sheet of the sandwich composite as an isotropic plate. Compressive fiber failure is highest at the center of the face sheet (Fig. 18b) as the center of the face sheet experiences maximum pressure as also shown in [18]. Matrix crack patterns are a result of strains experienced by the face sheet, and the matrix being weaker of the two constituents (i.e. fiber and matrix) cracks readily (Fig. 18c). Delamination i.e. failure between the fiber and matrix is shown in Fig. 18d. In the simulation, delamination is considered by incorporating Coulomb-Mohr theory (Equation 18) in material model 161.

The study by Hanssen *et al*. [6] reported that a cover plate in front of the foam results in 'dishing' (double/concave curvature) under blast loading. The study concluded that because of dishing, the foam can sustain a higher blast load. Dishing was also observed in the simulation in the present study as shown in Fig. 19. The dishing increased with increase in blast load. The displacement acquired by Face sheet2 (Fig. 20) in the direction of blast represents dishing. For e.g. blast was applied in the z-direction, hence the displacement of Face sheet2 (Fig. 19) in the z-direction represents dishing. The extent of dishing under various blast loads is shown in Fig. 20. The simulation was stopped when dishing started to decrease. It can be observed that highest dishing was observed in the case of 1 kg of TNT. The internal energy of foam for different loads is shown in Fig. 21. It can be seen that internal energy of the foam is maximum for 1 kg of TNT.

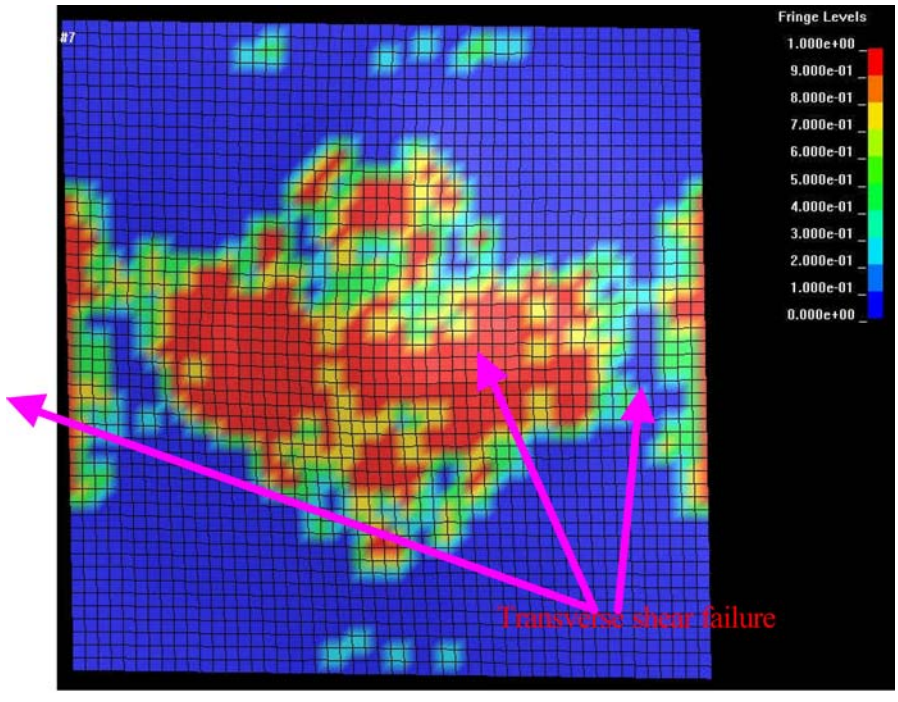


(a)

*Figure 18* (a) Shear mode failure in Face sheet1 at time of 1 ms, blast load = 5 MPa (0 = elastic & 1 = failure). (b) Compressive mode failure in Face sheet1 at time of 1 ms, blast load = 5 MPa (0 = elastic & 1 = failure). (c) Matrix cracking in Face sheet1 at time of 1 ms, blast load = 5 MPa (0 = elastic & 1 = failure). (d) Delamination in Face sheet1 at time of 1 ms, blast load = 5 MPa (0 = elastic & 1 = failure).

(*Continued on next page*)

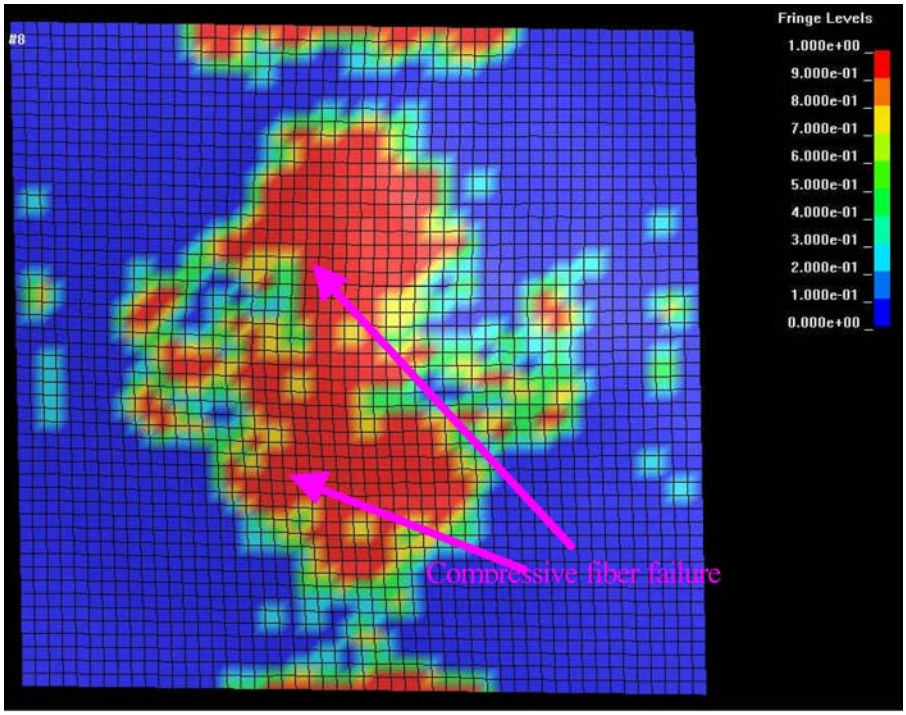


(b)

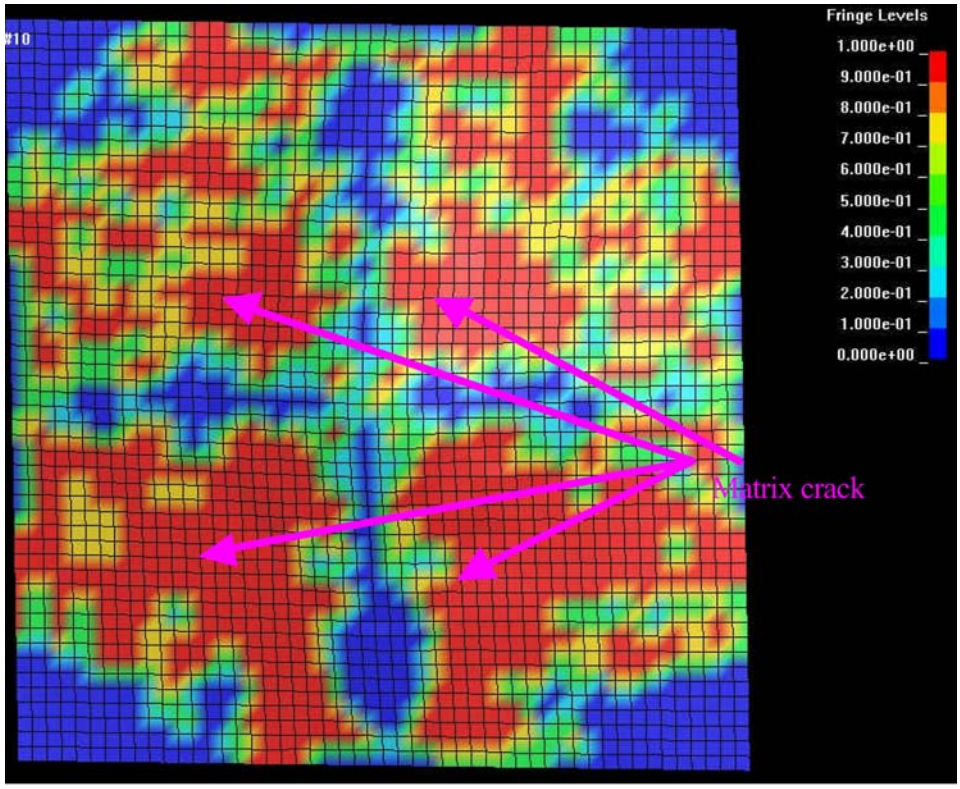


(c)

*Figure 18* (*Continued on next page*)

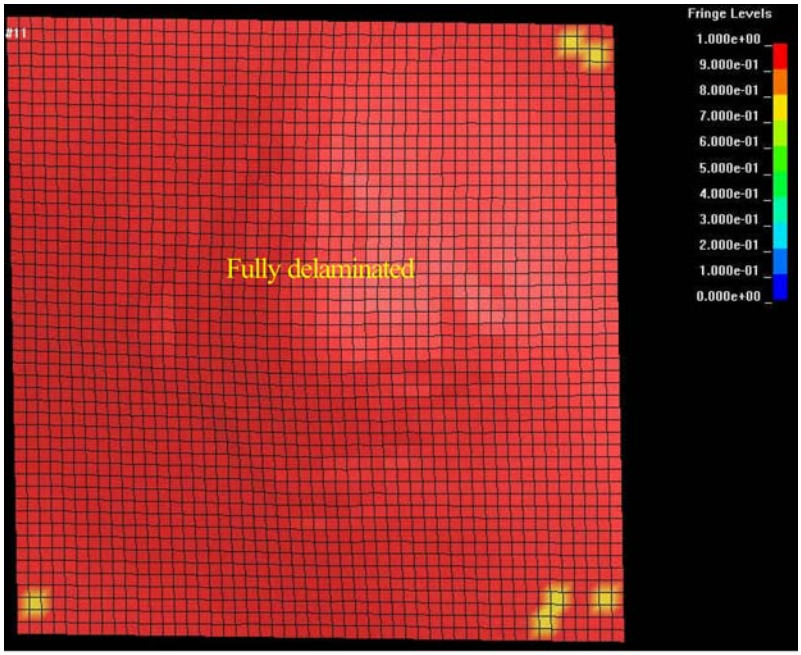


(d)

*Figure 18* (Continued)

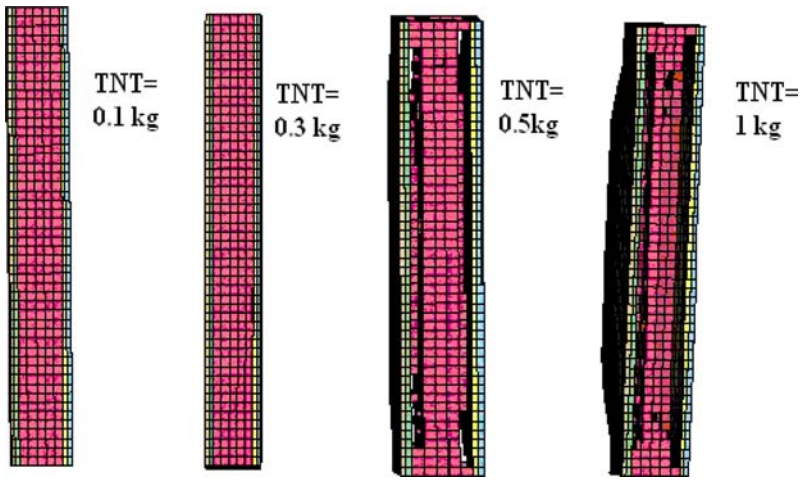


*Figure 19* Sandwich composite showing dishing at $t = 1$ ms for different loads of TNT placed 1 m away from sandwich composite.

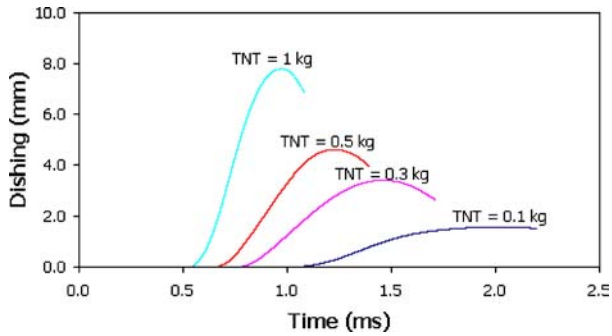


*Figure 20* Dishing of Face sheet2 under different loads of TNT was placed 1 m away from sandwich composite.

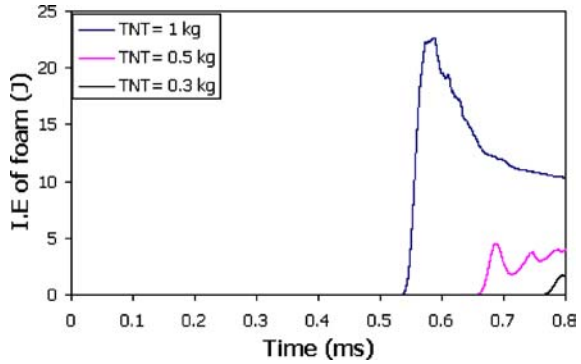


*Figure 21* Internal energy of the foam under different load of TNT placed 1 m away from sandwich composite.

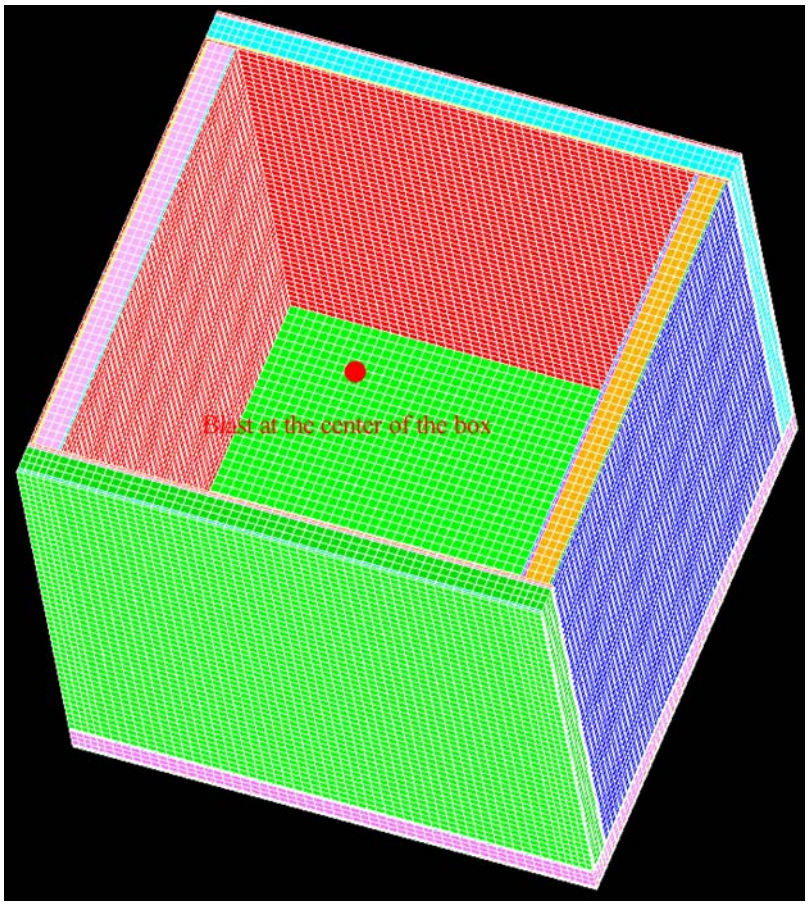


*Figure 22* Box made of sandwich composite.

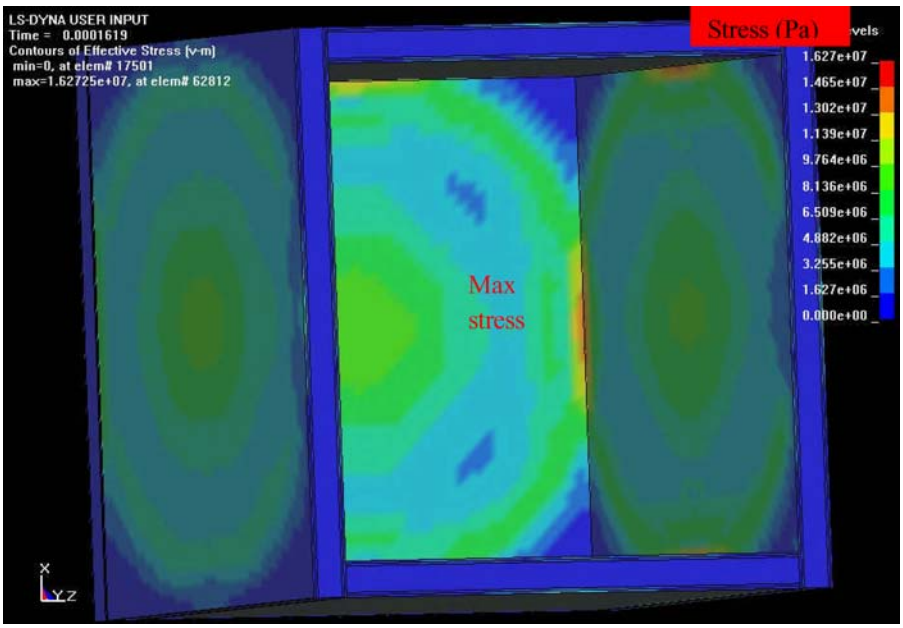


*Figure 23* Effect of 5 MPa on the sandwich composite box showing maximum stress at the corners.

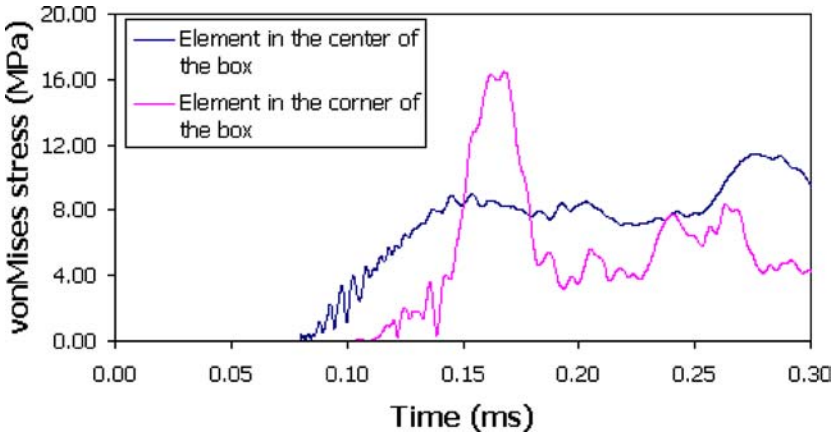


*Figure 24* Effect of 5 MPa blast load: comparison between the stress in the center and corner of the box.

The dishing of S2-glass/epoxy laminates subjected to blast load was observed to be similar to that reported in [9]. Using this concept as a basis, a box made of a sandwich composite with aluminum foam core and S2-glass/epoxy face sheets was analyzed for its blast response.

### 4.4. Blast impact on sandwich composite box

The sandwich composite box was modeled as plates of two face sheets on either side of the foam. The sandwich plates were assumed to be joined to form a cube-shaped box. The interior dimensions of the box were 0.3 m $\times$ 0.3 m $\times$ 0.3 m. The thickness of the core was 0.0159 m and the thickness of each face sheet was 0.0015 m. As discussed in the previous section, the blast load produced by 1 kg of TNT at 1 m distance from the sandwich plate was found to be 5 MPa. Hence a blast load of 5 MPa peak overpressure was applied on all sides of the box. The model for the box is shown in Fig. 22 and the effect of the blast load is shown in Fig. 23.

The blast wave reaches each face and produces a radial wavefront as shown in Fig. 23. The stress increases radially and maximum stress was observed at the corners. Constructive interference of wave front resulting from the blast causes maximum stress at the corners. The stress on an element in the middle of the face was compared to that of an element in the corner as shown in Fig. 24. The maximum von Mises stress on an element in the middle and corner of the box was 8.6 MPa and 16 Mpa, respectively. This implies that maximum stress is seen at the corners.

## 5. Summary

The present study relates to blast-resistant protective structures that can be made from lightweight composite face sheets and aluminum foam sandwich composites. Sandwich composite plate and a box made of S2-glass/epoxy laminated face sheets and aluminum foam core was simulated for blast loading in LS-DYNA. The blast loads excited at the geometric center of the plate and the box resulted in outward radial wave propagation. The damage progression of the sandwich composite occurred by 'dishing', which increased with increasing magnitude of the blast. These findings are consistent with studies of Hanssen *et al.* [6] who reported that 'dishing' causes increased energy transfer and better utilization of aluminum foam when a steel cover plate was used in front of aluminium foam. In the sandwich composite design, similar benefits of spreading the load from the face sheets to the aluminum can be attained. For the sandwich box (cube) the analysis predicted that the vulnerable locations are the joint locations of the box. Maximum stresses were observed along the edges of the box indicating the need to provide excess reinforcement at the joints of the sandwich panel box.

## Acknowledgements

Support from Dr. Dana Grow, Sioux Manufacturing, North Dakota and the National Science Foundation, DMI SBIR Award No. 0128164 & 0238614 is gratefully acknowledged

## References

1. D. J. HALL, *Composite Structures* **11** (1989) 101.
2. Z. XUE and J. W. HUTCHINSON, *International Journal of Mechanical Sciences* **45** (2003) 687.
3. M. O. CRITCHFIELD, T. D. JUDY and A. D. KURZWEIL, *Marine Structures* **7** (1994) 475.
4. M. F. ASHBY, A. G. EVANS, N. A. FLECK, L. J. GIBSON and J. W. HUTCHINSON, "Metal Foams: A Design Guide." (Butterworth-Heinemann, 2000).
5. A. G. EVANS, J. W. HUTCHINSON and M. F. ASHBY, *Progress in Materials Science* **43** (1999) 171.
6. A. G. HANSSEN, L. ENSTOCK and M. LANGSETH, *Int. J. Impact Eng.* **27** (2002) 593.
7. S. M. LIANG, L. N. WU and R. L. HSU, *Shock waves* **9** (1999) 367.

8. V. S. DESHPANDE and N. A. FLECK, *J. Mech. Phys. of Solids* **48** (2000a) 1253.
9. U. K. VAIDYA, S. PILLAY, C. A. ULVEN, A. R. S. GAUTAM, D. GROW and B. MATHEW, in Proceedings of the 14th International Conference on Composite Materials (ICCM/14), Paper ID EM03-332 (CD-ROM Proceedings, 2003).
10. J. BANHART, *Prog. Mater. Sci.* **46** (2001) 559.
11. CYMAT Technical Manual, Cymat Corp, Ontario, Canada (2004).
12. E. ANDREWS, W. SANDERS and L. J. GIBSON, *Mate. Sci. Eng. A* **270** (1999) 113.
13. P. H. THORNTON and C. L. MAGEE, *Metallur. Transac. A* **6A** (1975) 1253.
14. A. E. SIMONE AE and L. J. GIBSON, *Acta Materialia* **46** (1998b) 2139.
15. A. M. KRAYNIK and D. A. REINELT, *J. Colloid Interface Sci.* **181** (1996) 511.
16. L. D. KENNY, *Materials Science Forum* **217** (1996) 1183.
17. F. B. A. BESHARA, *Computers and Structures* (1994) 585.
18. G. RANDERS-PEHRSON and K. A. BANNISTER, ARL-TR-1310 (Army Research Laboratory, Aberdeen Proving Ground, 1997).
19. D. W. HYDE, SL-88-1 (U.S. Army Corps of Engineers Waterways Experiment Station Instruction, 1993).
20. C. N. KINGERY and G. BULMASH, ARBRL-TR-02555 (U.S. Army Ballistic Research Laboratory, Aberdeen Proving Ground, 1984).
21. W. ALTENHOF, A. M. HARTE and R. TURCHI, in Proceedings of the 7th International LS-DYNA Users Conference, May 2002, (Lawrence Livermore Technology Corporation and Engineering Technology Associates, Inc 2002) 13.
22. J. O. HALLQUIST, "LS-DYNA User's Manual." (Livermore Software Technology Corporation, 2004).
23. S. W. TSAI and E. M. WU, *J. Comp. Mater.* **5** (1971) 73.
24. Z. HASHIN, *J. Applied Mechanics* **47** (1980) 329.
25. LSTC help (ftp://ftp.lstc.com/outgoing/faq/, 2002).
26. C. F. YEN, in Proceedings of the 7th International LS-DYNA Users Conference, May 2002, (Lawrence Livermore Technology Corporation and Engineering Technology Associates, Inc 2002) 15.
27. S. BALA, *FEA Information International Newsletter* **8** (2001a) 8.
28. J. T. BEALS and M. S. THOMPSON, *J. Mater. Sci.* **32** (1997) 3595.
29. G. GIOUX, T. M. MCCORMACK and L. J. GIBSON, *Int. J. Mech. Sci.* **42** (2000) 1097.